# Higgs $\rightarrow ZZ^{(*)} \rightarrow 4l$ Analysis with DC1 Full ATLAS Simulation and Reconstruction

Stathes Paganis[†‡]

[†] *Department of Physics and Astronomy, The University of Sheffield, Sheffield, UK*

[‡] *Most of this work was performed while at the University of Wisconsin with Prof. Sau Lan Wu's Higgs group.*

**21 August 2005**

**Abstract**

In this note a combined Higgs $H \rightarrow ZZ^{(*)} \rightarrow 4l$ analysis using full ATLAS simulation and reconstruction and the Data Challenge 1 (DC1) detector layout, is presented. We follow closely the analysis performed in the ATLAS Technical Desing Report (TDR) attempting to examine the effects of the new ATLAS layout and offline reconstruction on the analysis performance. This study finds **no significant loss of sensitivity due to the increase of material upstream of the LAr Calorimeter**. The 10-15% drop in signal yield with respect to the ATLAS TDR at low Higgs masses was traced in electron and muon efficiency losses during the isolation and impact parameter cut steps. For electrons, the calorimeter isolation cuts were optimized for $p_{\perp} \geq 20$ GeV, thus a reoptimization of these cuts below 20 GeV is expected to recover a large part of this loss. Efficiency loss in the electron impact parameter cut is also expected since tracking must be optimized for the increased Bremsstrahlung levels. For muons the loss is attributed to two factors: the absense of a refined Impact Parameter cut which takes into account the spread of the primary vertex in the transverse plane, and the absense of Calorimetric isolation cuts (our samples had no electronic noise). These cuts were used in the ATLAS TDR giving a 10-20% increase in the $H \rightarrow 4\mu$ efficiency for the same reducible background rejection.

# Contents

# 1 Introduction

The observation of a Higgs boson in ATLAS through its $H \to ZZ^{(*)} \to 4l$ decay mode, has been studied in detail since the early-90's [1]. For a large part of the possible Higgs mass range, this channel provides in the invariant mass of the 4-leptons, a narrow peak on top of a smooth background. In addition, tight isolation cuts on the leptons lead to a large Signal to Background ratio, making the $H \to ZZ^{(*)} \to 4l$ a *golden channel* for discovering the Higgs at LHC.

In this note a combined Higgs $H \to ZZ^{(*)} \to 4l$ analysis using full ATLAS simulation and reconstruction and the Data Challenge 1 (DC1) detector layout, is presented. The main goal of this analysis is to revisit the ATLAS Technical Desing Report (TDR) analysis strategy for this channel [2], using the latest reconstruction software. Moreover one would like to study the effects of the new ATLAS layout (increase of the material upstream of the EM Calorimeter) on the $H \to ZZ^{(*)} \to 4l$ analysis performance. Identification of a possible performance deterioration at a particular step of this analysis, would help us define the reconstruction areas which we will have to improve in the future. For these reasons, the analysis strategy applied here closely resembles the analysis performed in the ATLAS TDR.

The note is structured as follows: first the Monte Carlo (MC) samples are described. Then the lepton reconstruction is discussed. Finally the results of the $H \to ZZ^{(*)} \to 4l$ analysis are presented and compared to the ATLAS TDR [2].

It should be mentioned that during the course of this work an electron specific longitudinal weight extraction was performed, using a parametrization motivated by recent ATLAS Test-Beam analyses. This is the subject of a different note [3]. Electron calibration, electron efficiency and Higgs reconstruction performance results are given in an appendix.

# 2 Monte-Carlo Sample Production

A large set of MC data samples was generated for the purposes of this analysis. The full set of MC files is presented in table 1.

The generation definition for the standard Higgs and background samples ($pp \to ZZ \to 4l$) is summarized below:

- Generation in Athena 6.5.0, using Pythia 6.203 [4] and a 4 final state electron filter using a modified MultiLeptonFilter.
- Simulation using Atlsim 01-03-08 (Geant 3.21).
- Cuts in the particle level filter at $|\eta| \leq 2.7$, $p_\perp > 4$ GeV (for 4 electrons).

Table 1: *Fully Simulated and Reconstructed Monte Carlo files used in this analysis*

| Channel | Run Number | Events | Passed Filter | Gen./Sim. V. | Recon. V. |
|---|---|---|---|---|---|
| H(130GeV)$\rightarrow 4e$ | 2505 | 100k | 63684 | 6.5.0/6.5.0 | 6.5.3 |
| H(150GeV)$\rightarrow 4e$ | 2506 | 100k | 65000 | 6.5.0/6.5.0 | 6.5.3 |
| H(180GeV)$\rightarrow 4e$ | 2507 | 100k | 71618 | 6.5.0/6.5.0 | 6.5.3 |
| H(200GeV)$\rightarrow 4e$ | 2541 | 100k | 73549 | 6.5.0/6.5.0 | 6.5.3 |
| H(300GeV)$\rightarrow 4e$ | 2542 | 100k | 77241 | 6.5.0/6.5.0 | 6.5.3 |
| $pp \rightarrow ZZ \rightarrow 4l$ | 2648 | 12.5M | 559707 | 6.5.0/7.0.2 | 7.0.2 |
| $gg \rightarrow Zb\bar{b} \rightarrow 4e$ | 2658 | 120M | 568k | 6.5.0/6.5.0 | 7.0.2 |
| $gg \rightarrow Zb\bar{b} \rightarrow 2e2\mu$ | 2659 | | | | |
| $gg \rightarrow Zb\bar{b} \rightarrow 4\mu$ | 2346 | | | | |
| $gg \rightarrow t\bar{t} \rightarrow 4e$ | 2599 | 5.58M | 43361 | 7.0.0/6.5.0 | 6.0.3 |
| $gg \rightarrow t\bar{t} \rightarrow 2e2\mu$ | 2633 | N/A | 176542 | 7.0.0/6.5.0 | 6.0.3 |

- Cuts in the simulation at $|\eta| \leq 2.7$, (for 4 electrons).
- Reconstruction using Athena 6.5.3 for signal, and 7.0.2 for background (for $t\bar{t}$ see below). The standard e/$\gamma$ job options for low luminosity were used. Electronic noise in the CALO was switched off. No pile-up was added.
- For the $4\mu$ final state the Data Challenge 1 (DC1) samples were used [7].

Samples were also generated at Next-to-Leading Order (NLO) for Higgs and background ($t\bar{t}$ ):

- Generation in Athena 7.0.0, using Herwig [6] and MC@NLO [5], and filtering in the final state using a modified MultiLeptonFilter.
- Simulation using Atlsim 01-03-08 (Geant 3.21).
- Cuts in the particle level filter $|\eta| \leq 2.7$, $p_{\perp} > 4$ GeV (for 4 electrons).
- Cuts in the detector simulation at $|\eta| \leq 2.7$, (for 4 electrons).
- Reconstruction using Athena 6.0.3, with the e/$\gamma$ eg9.lumi02.603.job options (Standard e/$\gamma$ job options, low luminosity).

The EMShowerBuilder algorithm in Athena was modified so that the low luminosity shower cuts in EM identification are applied.

# 3 Reconstruction and Performance

In this section the necessary definitions for the leptons are listed. In the case of electrons a calculation of optimum longitudinal weights was performed. Starting with Data Challenge 2 (DC2), the method used in this note became the default in ATLAS and optimum weights for the Barrel and EndCap are provided by the *egamma* group. For completion, the calibration and efficiency for electrons (including FEE noise and pile-up) are presented.

## 3.1 Definitions for Electrons

The electrons used in this analysis originate from *egamma* objects in the ATLAS nomenclature. These objects are included in the *egamma* block of the DC1 CBNT ntuple and are built from Liquid Argon (LAr) Calorimeter information. They are candidate electrons since no eletromagnetic identification criteria have been applied yet and no associated tracks have been required. Below we give a list of the characteristics of the *egamma* objects:

- Clustering: fixed size 3×7 using a sliding window algorithm.
- Cluster Energy Threshold: 3 GeV.
- Efficiency: $\geq$ 99% (see Fig. 9).
- Associated Track Information: *egamma* clusters have pointers to one associated track. The efficiency of the track/cluster matching is $\simeq$ 92%.
- Shower Shape information: the *egamma* objects contain detailed shower shape information which is typically used for separating an electromagnetic cluster from a hadronic cluster.
- EM isolation information: a set of cuts described in [3], [8], are applied to *egamma* objects, to define the level of their isolation. Based on these cuts an id flag called *eg_ISEM* is filled. This EM isolation step is part of the ATLAS offline reconstruction.
- Cluster corrections: the *egamma* clusters have gone through a number of cluster level corrections for position and energy modulations, out-of-cluster cone corrections and intercryostat gap energy losses.

The definition of an electron used in this analysis requires the following:

- An *egamma* cluster.
- A cluster/track match.

- An isolated cluster (eg_ISEM= 0).
- $E/p < 2.3$
- At least 9 Silicon detector hits.
- A cluster/track $E_\perp$ optimal combination was performed following the ATLAS TDR. The details and performance of the combination are discussed in [3].

### 3.2 Definitions for Muons

The muons used in this analysis originate from the muon combined block contained in the DC1 CBNT. The combined block contains muon candidates from the muon chambers which were matched and refitted to Inner Detector (ID) tracks. The quality of the refit is encoded in a quality flag called: *fitcodecb*.

The definition of a muon used in this analysis requires the following:

- A combined *cb* muon.
- A high quality refitted *cb* muon (fitcodecb= 0).

### 3.3 Calibration for electrons

A test beam motivated method to extract longitudinal weights for electrons is described in [3]. The purpose of these weights is to provide best linearity and resolution for electrons of energies ranging from 10 GeV to the TeV scale. The effect of these weights on electrons and in particular on the Higgs invariant mass are summarized in the appendix. A direct comparison with the ATLAS TDR shows a $\simeq$ 10% degradation of the Higgs mass resolution at low masses. This small degradation is attributed to (i) the increased amount of material upstream the EM Calorimeter which results in an increase in the Bremsstrahlung tails in the electron energy reconstruction, and (ii) the fact that the longitudinal weights were extracted only for the Barrel excluding the crack region (electrons with $|\eta| > 1.37$ have worse resolution than in the TDR).

### 3.4 Efficiency for electrons including FEE noise and pile-up

A study of single electron efficiency after each step of the preselection used in this analysis, is presented in an appendix. In this study FEE noise and physics pile-up corresponding to a luminosity of $2.10^{33} cm^{-2} s^{-1}$ were included. The efficiency after all cuts depends on the electron $p_\perp$ dropping significantly for $p_\perp < 20$ GeV. The overall single electron efficiency after all quality cuts is energy and $\eta$ dependent. It ranges from $\simeq$80% at 15 GeV to a flat $\simeq$90% at higher energies in the Barrel. In the Endcap and for $\eta > 1.8$ the efficiency drops by about 10% with respect to the barrel (Fig. 13).

# 4 Higgs→4l Analysis

The search for Higgs→4l decays at LHC requires two different analysis strategies due to the dependence of the signal and background cross-sections and branching rations (BR) on the Higgs mass. For Higgs masses below the $ZZ$ threshold $\simeq$ (182 GeV), the signal (cross-section×BR) is significantly smaller due to the small $H \rightarrow ZZ^{(*)}$ branching ratio. This is shown in Table 2 for a LO calculation of the cross-section [4].

Table 2: *Higgs→ 4lepton LO cross-sections× BR used in this analysis. The total cross sections used in the ATLAS TDR are shown in parenthesis for reference.*

| Higgs Mass (GeV) | 130 | 150 | 180 | 200 | 300 |
|---|---|---|---|---|---|
| Cross section $pp \rightarrow H$ (pb) | 20.75 | 16.35 | 12.04 | 10.07 | 5.40 |
| (TDR Cross section $pp \rightarrow H$) | (18.8) | (15.4) | (12.9) | N/A | N/A |
| Branch. Ratio $H \rightarrow ZZ$ | 0.03841 | 0.08284 | 0.05750 | 0.2613 | 0.3075 |
| Branch. Ratio $ZZ \rightarrow 4l$ | 0.004532 | 0.004532 | 0.004532 | 0.004532 | 0.004532 |
| Cross section×BR (fb) | 3.61 | 6.138 | 3.1375 | 11.92 | 7.525 |

In addition the reducible background cross-section (mainly $Zb\overline{b}$ and $t\bar{t}$ ) is very large at the low $ZZ$ mass region requiring tight lepton isolation cuts for its removal.

## 4.1 Electron Isolation

Electron isolation is applied in two steps following the TDR approach. First, as discussed in section 3, a LAr Calorimetric isolation is applied where a number of shower shape cuts are applied in sequence and the results of these cuts are encoded in variable *eg_ISEM*. The isolation cuts are discussed in [3] and in references therein. They consist of three steps, a requirement of small leakage in the hadronic calorimeter, a set of cuts using second (middle) sampling shower shape variables, and cuts on shower shapes which come from the first (strip) sampling. Secondly, an Inner Detector isolation is applied in which the sum of the $p_\perp$ of tracks contained in a cone of $\Delta R \leq 0.2$ around the electron track, is required to be less than 10 GeV (Figure 1). Finally, an impact parameter cut is applied to reject background leptons which come b-quarks (Figure 2).

The background rejection versus signal efficiency for the isolation cuts presented in this analysis are summarized in table 3, for 130 GeV Higgs mass. From the table it is clear that for a 1200 rejection for the $t\bar{t}$ background we will have a 0.46 efficiency which is significantly lower than what was obtained in the ATLAS TDR. However the situation improves for higher masses as shown later in the full efficiency table 6. This efficiency drop will have an impact on the final results obtained in this note. Our approach in this analysis is to choose the cuts so that the $t\bar{t}$ rejection is $\simeq$ 1200.

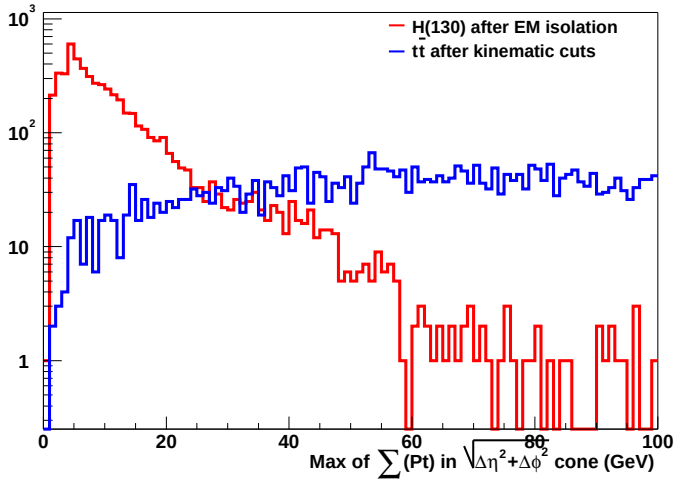


Figure 1: Inner Detector lepton isolation: distribution of $\sum p_\perp$ within a cone of $\sqrt{\Delta\eta^2 + \Delta\phi^2} \leq 0.2$.

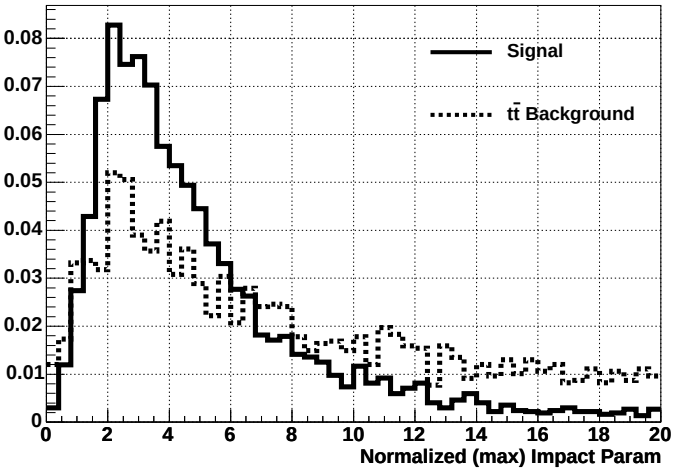


Figure 2: Impact Parameter Cut for electrons.

Table 3: *Electron Isolation Performance*

| Cut | $t\bar{t}$ rejection | $H \to 4e$ efficiency |
|---|---|---|
| Leakage + 2nd Sampl. + 1st Sampl. | 123 ±10 | 0.61 |
| Leakage + 2nd Sampl. | 59.5±3.3 | 0.73 |
| Leakage | 11 | 0.86 |
| Inner Detector $\sum p_\perp \leq$ 10GeV | 45±2 | 0.81 |
| Combined EM+ID | 418±61 | 0.56 |
| Combined EM+ID+Impact Parameter | 1155±280 | 0.46 |

## 4.2 Muon Isolation

Isolation cuts must be applied for muons but in this case the calorimeter cuts are not applied on shower shapes, but instead on energy deposition inside a cone around the muon track. The determination of the optimum cone size depends critically on the electronics noise and pile-up. Presently we are simulating and reconstructing events without these two effects. Consequently we prefer not to perform a calorimeter isolation following a more conservative approach. For muon isolation we will rely only on ID tracking information and will apply a cut on the energy inside a cone around the muon the same way we did for the electrons. An impact parameter cut is also applied for the muons.

## 4.3 $Z \to ee$ mass constraint: Higgs Mass resolution and efficiency

The impact of a $Z \to ee$ constrained fit on the Higgs mass resolution is shown in Fig. 3, for a Higgs mass of 130 GeV. The constrained fit reduces by 10-15% the width of the mass distribution.

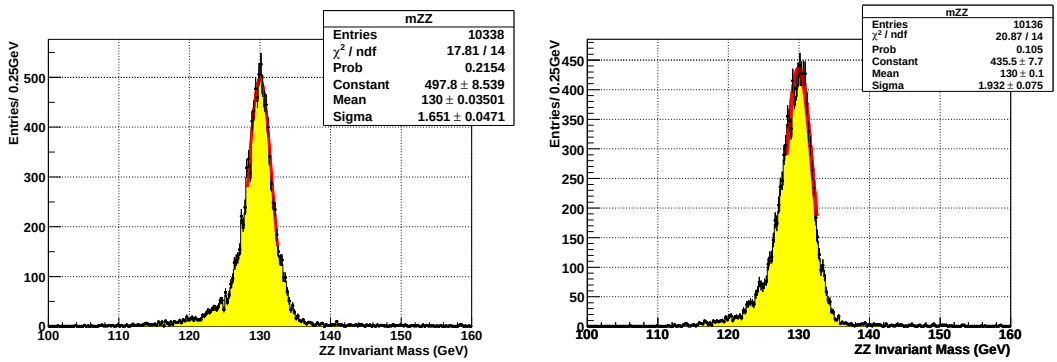


Figure 3: Higgs mass resolution with (left plot) and without (right plot) $Z \to ee$ constrained fit, for a Higgs mass of 130GeV.

The Higgs mass resolution versus the Higgs mass is shown in Fig. 4. The effect of the constrained fit on the efficiency is relatively small (1-2%) due to the wide Higgs mass window cut applied in a TDR-based analysis (see Table 5).

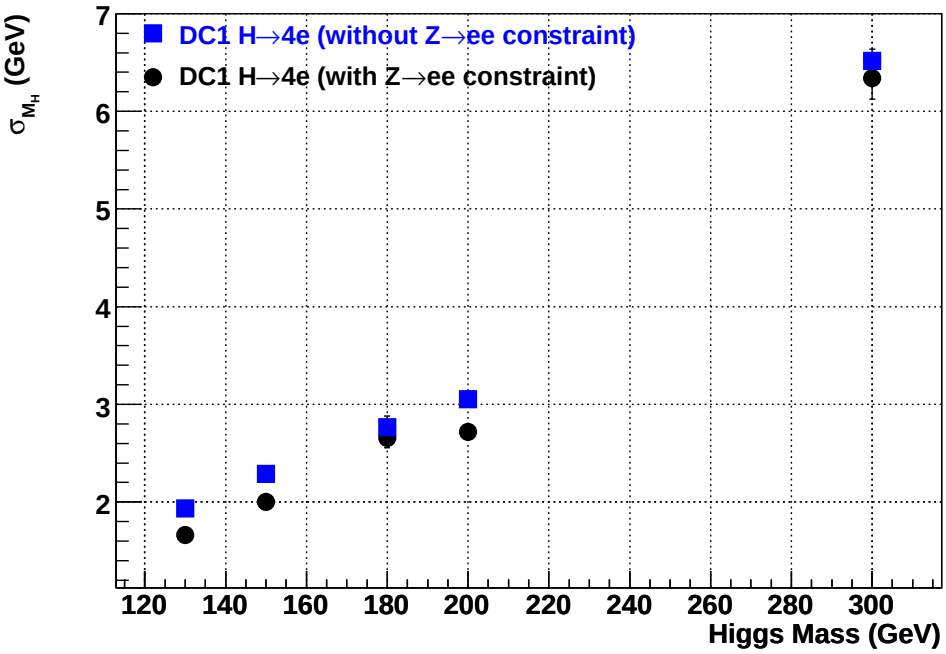


Figure 4: Higgs mass resolution as a function of the Higgs mass with (blue circles) and without (black squares) $Z \to ee$ constraint fit.

Table 4: *Higgs→4e Selection Cut Efficiency*

| Selection Cuts | 130 | 150 | 180 |
|---|---|---|---|
| Total Efficiency (with constraint) | 0.096 | 0.130 | 0.163 |
| Total Efficiency (no constraint) | 0.094 | 0.127 | 0.162 |

### 4.4 Higgs→4e Analysis

A description of the selection cuts for the Higgs→4e analysis follows:

1. Lepton filter: 4 particle level electrons with $\eta \leq 2.7$, $p_\perp > 4$ GeV.
2. Offline Trigger (TDR): 4 electrons as defined in section 3, with $p_\perp > 7$ GeV,

$\eta \leq 2.5$ and at least 2 of them with $p_\perp > 20$ GeV. The electron definition is repeated below:

- All candidate electrons are *egamma* objects (section 3).
- Matching: each candidate electron should have a single ID track associated (matched) to it during reconstruction.
- Quality: At least 9 hits in the Silicon Detectors and $E/p < 2.3$.
- EM cluster isolation: each candidate electron must pass the official EM shower isolation criteria encoded in eg_ISEM= 0.
- A cluster/track $E_\perp$ optimal combination was performed following the ATLAS TDR [3].

3. ID isolation: the sum of the $p_\perp$ of tracks contained in a cone of $\Delta R \leq 0.2$ around the electron track should be less than 10 GeV.
4. Impact parameter cut: the normalized distance of closest approach (DCA) of an electron to the IP should not be larger than 10 $\sigma$, where $\sigma$ is the total error in the extraction of the DCA.
5. $ZZ^{(*)}$ mass cuts (TDR): the cuts are described in table 5.
6. Higgs Mass Window: the cuts are described in table 5.

Table 5: *Higgs→4l mass cuts (common to all analyses)*

| Selection Cuts | 130 | 150 | 180 | 200 | 300 |
|---|---|---|---|---|---|
| $Z$ mass cuts $91.18 \pm \Delta M$ (GeV) | $\pm 15$ | $\pm 10$ | $\pm 6$ | $\pm 6$ | $\pm 6$ |
| $Z^{(*)}$ mass cuts (min,max) (GeV) | 20, 111 | 30, 111 | 60, 111 | $\pm 6$ | $\pm 6$ |
| H Mass Window $M_H \pm \Delta M$ (GeV) | $\pm 5$ | $\pm 5$ | $\pm 5$ | $\pm 6.634$ | $\pm 11.476$ |

The Higgs→4e efficiency after each cut is shown in table 6. The first row shows the Generator Filter efficiency. The second row gives the efficiency of events with four electrons that are matched to tracks. From these numbers one can extract a $\simeq 92\%$ efficiency for electrons which are required to have a track matched to them. The third row shows the portion of events which pass the offline trigger. The rest of the information in the table is self-explanatory.

A comparison with the TDR (tables 19-12, 19-13) shows similar efficiencies for all steps except the EMC isolation and impact parameter steps where our analysis shows a significant drop in efficiency (10-20%). The EMC isolation cuts were optimized for $p_\perp \geq 20$ GeV and in the low Higgs mass region the majority of the softest electrons have $p_\perp < 20$ GeV. A reoptimization of these cuts below 20 GeV is expected to recover most of the loss. The increase in the amount of material upstream of the LAr Calorimeter should increase the level of Bremsstrahlung for electrons, requiring an optimization of

the tracking algorithms which will improve the impact parameter resolution. Presently this is not the case and a loss of efficiency in the impact parameter cut for electrons is expected.

Table 6: *Higgs→4e Selection Cut Efficiency*

| Selection Cuts | 130 | 150 | 180 | 200 | 300 |
|---|---|---|---|---|---|
| Filter Efficiency | 0.64 | 0.65 | 0.72 | 0.74 | 0.77 |
| $\geq$ 4 track-matched e, no cuts | 0.65 | 0.70 | 0.73 | 0.74 | 0.77 |
| $\geq$ 4 track-matched e, $\eta$ and $p_\perp$ cut | 0.84 | 0.92 | 0.96 | 0.96 | 0.97 |
| EMC Isolation | 0.56 | 0.60 | 0.64 | N/A | N/A |
| ID Isolation | 0.91 | 0.90 | 0.89 | N/A | N/A |
| Impact Parameter cut | 0.84 | 0.84 | 0.85 | N/A | N/A |
| $ZZ^{(*)}$ mass cuts | 0.70 | 0.75 | 0.80 | 0.59 | 0.60 |
| Higgs Mass Window | 0.92 | 0.92 | 0.84 | 0.93 | 0.76 |
| Total | 0.096 | 0.13 | 0.16 | 0.29 | 0.26 |

The Poisson significance for the $H \rightarrow$4e channel for 30 fb$^{-1}$ using full ATLAS simulation and reconstruction is presented in table 7.

Table 7: *Higgs→4e TDR-based Analysis Summary*

| Higgs Mass (GeV) | 130 | 150 | 180 | 200 | 300 |
|---|---|---|---|---|---|
| Cross section×BR (fb) | 0.903 | 1.5346 | 0.7844 | 2.9812 | 1.8813 |
| Signal (fb) | 0.0858 | 0.1999 | 0.1271 | 0.5914 | 0.3424 |
| pp→ZZ$^{(*)}$ →4e (fb) | 0.0209 | 0.0154 | 0.0789 | 0.2244 | 0.0940 |
| pp→$t\bar{t}$ →4e (fb) | 0.005 | <0.005 | <0.005 | <0.005 | <0.005 |
| gg→Z$b\bar{b}$ →4e (fb) | 0.0094 | 0.0036 | 0.0014 | <0.001 | <0.001 |
| 30 fb$^{-1}$ Signal | 2.574 | 5.997 | 3.813 | 17.742 | 10.272 |
| 30 fb$^{-1}$ Bgnd | 1.059 | 0.72 | 2.559 | 6.912 | 3.0 |
| Significance | 1.33 | 4.25 | 1.68 | 4.98 | 4.16 |

### 4.5 Higgs→2e2$\mu$ Analysis

A description of the selection cuts for the Higgs→2e2$\mu$ analysis follows:

1. Lepton filter: 2 particle level electrons and 2 muons with $\eta \leq 2.7$, $p_\perp > 4$ GeV.
2. Reconstructed electrons: 2 EM clusters each having a single ID track associated (matched) to it during reconstruction.

3. Offline Trigger (TDR): 2 electrons and 2 muons, as defined in section 3, with $p_\perp > 7$ GeV, $\eta \leq 2.5$ and at least 2 of them with $p_\perp > 20$ GeV.

4. EMC isolation: each electron must have $eg\_ISEM = 0$.

5. ID isolation: the sum of the $p_\perp$ of tracks contained in a cone of $\Delta R \leq 0.2$ around the electron track should be less than 10 GeV, and around the muon track should be less than 5 GeV.

6. Impact parameter cut: the normalized distance of closest approach (DCA) of a track to the IP should not be larger than 5 $\sigma$ for electrons and 3.5 $\sigma$ for muons, where $\sigma$ is the total error in the extraction of the DCA.

7. $ZZ^{(*)}$ mass cuts (TDR): the cuts are described in table 5.

8. Higgs Mass Window: the cuts are described in table 5.

The Poisson significance for the $H \rightarrow$2e2$\mu$ channel for 30 fb$^{-1}$ using full ATLAS simulation and reconstruction is presented in table 8.

Table 8: *Higgs→2e2μ TDR-based Analysis Summary*

| Higgs Mass (GeV) | 130 | 150 | 180 | 200 | 300 |
|---|---|---|---|---|---|
| Cross section×BR (fb) | 1.806 | 3.0692 | 1.5688 | 5.9624 | 3.7626 |
| Signal (fb) | 0.154 | 0.362 | 0.265 | 1.402 | 0.901 |
| pp→ZZ$^{(*)}$ →2e2$\mu$ (fb) | 0.032 | 0.0267 | 0.1255 | 0.62 | 0.252 |
| pp→$t\bar{t}$ →2e2$\mu$ (fb) | <0.002 | <0.002 | <0.002 | 0.058 | 0.014 |
| gg→Z$b\bar{b}$ →2e2$\mu$ (fb) | 0.007 | 0.0014 | 0.001 | 0.057 | 0.03152 |
| 30 fb$^{-1}$ Signal | 4.62 | 10.86 | 7.95 | 42.06 | 27.03 |
| 30 fb$^{-1}$ Bgnd | 1.23 | 0.9 | 3.855 | 22.05 | 8.9256 |
| Significance | 2.93 | 6.21 | 3.21 | 7.20 | 6.74 |

### 4.6 Higgs→4$\mu$ Analysis

A description of the selection cuts for the Higgs→4$\mu$ analysis follows:

1. Lepton filter: 4 particle level muons with $\eta \leq 2.7$, $p_\perp > 4$ GeV.

2. Reconstructed muons: 4 muons at the combined muon block in CBNT.

3. Offline Trigger (TDR): 4 muons, as defined in section 3, with $p_\perp > 7$ GeV, $\eta \leq 2.5$ and at least 2 of them with $p_\perp > 20$ GeV.

4. EMC isolation: not applied.

5. ID isolation: the sum of the $p_\perp$ of tracks contained in a cone of $\Delta R \leq 0.2$ around the muon track should be less than 5 GeV.

6. Impact parameter cut: the normalized distance of closest approach (DCA) of a muon to the IP should not be larger than 3.5 $\sigma$, where $\sigma$ is the total error in the extraction of the DCA.

7. $ZZ^{(*)}$ mass cuts (TDR): the cuts are described in table 5.

8. Higgs Mass Window: the cuts are described in table 5.

The Higgs$\rightarrow 4\mu$ efficiency after each cut is shown in table 9. The first row is similar to the one obtained in the 4e analysis and since there is no track-cluster matching, the second row here should be compared to the product of the second and third rows from the 4e analysis (table 6).

The efficiencies obtained here for the combined isolation and impact parameter cuts can be directly compared to the ones in the ATLAS TDR. A 15-20% drop in efficiency is seen (similar to the drop seen in the 4e case). However, here the drop in efficiency can be attributed, first, to the absence of a refined Impact Parameter cut (SUMDI) which corrects for the spread of the primary vertex in x and y (a 10-15% effect) and second, to the absense of calorimetric isolation cuts. In fact we should not expect dramatic changes in the muon efficiencies since the increase of material in the new ATLAS layout should have no impact in their reconstruction.

Table 9: *Higgs$\rightarrow 4\mu$ Selection Cut Efficiency*

| Selection Cuts | 130 | 150 | 180 | 200 | 300 |
|---|---|---|---|---|---|
| Filter Efficiency | 0.65 | 0.69 | 0.73 | 0.75 | 0.78 |
| $\geq 4\mu$ $\eta$ and $p_\perp$ cut | 0.58 | 0.65 | 0.70 | 0.69 | 0.72 |
| EMC Isolation | N/A | N/A | N/A | N/A | N/A |
| ID Isolation | 0.80 | 0.84 | 0.84 | 0.85 | 0.85 |
| Impact Parameter cut | 0.80 | 0.82 | 0.85 | 0.85 | 0.87 |
| $ZZ^{(*)}$ mass cuts | 0.70 | 0.71 | 0.77 | 0.61 | 0.57 |
| Higgs Mass Window | 0.90 | 0.87 | 0.78 | 0.90 | 0.73 |
| Total | 0.15 | 0.19 | 0.22 | 0.21 | 0.18 |

The Poisson significance for the $H \rightarrow 4\mu$ channel for 30 fb$^{-1}$ using full ATLAS simulation and reconstruction is presented in table 10.

### 4.7 Combined Analysis

The results of the individual $ZZ \rightarrow 4e$, $ZZ \rightarrow 2e2\mu$ and $ZZ \rightarrow 4\mu$ analyses can be statistically combined to provide the final result for the $H \rightarrow 4l$ analysis. The

Table 10: *Higgs→4μ TDR-based Analysis Summary*

| Higgs Mass (GeV) | 130 | 150 | 180 | 200 | 300 |
|---|---|---|---|---|---|
| Cross section×BR (fb) | 0.903 | 1.5346 | 0.7844 | 2.9812 | 1.8813 |
| Signal (fb) | 0.1367 | 0.296 | 0.171 | 0.612 | 0.329 |
| pp→ZZ$^{(*)}$ →4$\mu$ (fb) | 0.031 | 0.029 | 0.09546 | 0.24166 | 0.098 |
| pp→$t\bar{t}$ →4$\mu$ (fb) | 0.0 | 0.0 | 0.0 | 0.0 | 0.0 |
| gg→Z$b\bar{b}$ →4$\mu$ (fb) | 0.004 | <0.002 | <0.002 | <0.002 | <0.002 |
| pp→ZZ→2$\tau$2$\mu$ (fb) | 0.003 | 0.003 | 0.0007 | 0.0 | 0.0 |
| 30 fb$^{-1}$ Signal | 4.1 | 8.88 | 5.13 | 18.36 | 9.87 |
| 30 fb$^{-1}$ Bgnd | 1.14 | 1.02 | 2.945 | 7.31 | 3.0 |
| Significance | 2.50 | 5.15 | 2.30 | 5.27 | 4.16 |

final combined significance for the $H \rightarrow 4l$ channel using full ATLAS simulation and reconstruction is presented in table 11.

Table 11: *Higgs→4e,2e2μ,4μ TDR-based Combined Analysis Summary*

| Higgs Mass (GeV) | 130 | 150 | 180 | 200 | 300 |
|---|---|---|---|---|---|
| Cross section×BR (fb) | 3.61 | 6.138 | 3.1375 | 10.07 | 5.40 |
| 30 fb$^{-1}$ 4e Signal | 2.574 | 5.997 | 3.813 | 17.742 | 10.272 |
| 30 fb$^{-1}$ 4e Bgnd | 1.059 | 0.72 | 2.559 | 6.912 | 3.0 |
| 30 fb$^{-1}$ 2e2$\mu$ Signal | 4.62 | 10.86 | 7.95 | 42.06 | 27.03 |
| 30 fb$^{-1}$ 2e2$\mu$ Bgnd | 1.23 | 0.9 | 3.855 | 22.05 | 8.9256 |
| 30 fb$^{-1}$ 4$\mu$ Signal | 4.1 | 8.88 | 5.13 | 18.36 | 9.87 |
| 30 fb$^{-1}$ 4$\mu$ Bgnd | 1.14 | 1.02 | 2.945 | 7.31 | 3.0 |
| Significance (Lik.Ratio) | 4.52 | 9.12 | 4.51 | 10.22 | 8.94 |
| Significance (Quadrature) | 4.07 | 9.12 | 4.29 | 10.22 | 8.94 |

For completness a comparison between our result and the TDR result is presented in table 12. It should be noted that the cross-sections for signal and background used in the TDR are somewhat lower ( 10% than the ones used in this analysis) for Higgs masses 130 and 150GeV. For 180GeV the TDR cross-section is slightly higher. From this comparison we observe a decrease in the signal yield by 10-15% as compared to the TDR. This signal loss is consistent with the drop in signal efficiency in the isolation step for electrons (table 6), and muons (table 9). It is possible that this loss of efficiency can be recovered by reoptimizing the isolation cuts, in particular for electron $p_\perp$ in the region 7 GeV$\leq$ $p_\perp$ $\leq$ 20 GeV. Optimization in this region should also increase the background rejection.

From table 12 we also observe a particularly large increase of the background for the 180 GeV mass point. For a Higgs mass of 180 GeV we indeed expect an increase of the $ZZ^{(*)}$ irreducible background by a factor of 3. This is shown in figure 5 where the

Table 12: *Higgs→4e,2e2μ,4μ TDR-based Combined Analysis Summary*

| Higgs Mass (GeV) | 130 | 150 | 180 |
|---|---|---|---|
| 30 fb$^{-1}$ TDR Signal (events) | 11.4 | 26.8 | 19.7 |
| 30 fb$^{-1}$ This Analysis Signal (events) | 11.294 | 25.737 | 16.893 |
| 30 fb$^{-1}$ TDR Bgnd (events) | 2.61 | 2.98 | 3.1 |
| 30 fb$^{-1}$ This Analysis Bgnd (events) | 3.43 | 2.64 | 9.359 |

rapid increase of the background is due to the turn-on of on-shell $ZZ$ pairs close to the $ZZ$ threshold.

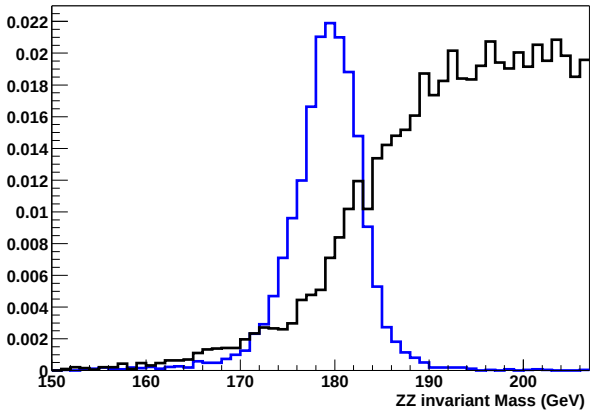


Figure 5: Invariant mass distribution of $H(180) \rightarrow ZZ \rightarrow 4e$ and $ZZ^{(*)} \rightarrow 4e$ irreducible background. The rapid increase of the background is due to the turn-on of true $ZZ$ pairs close to the $ZZ$ threshold (plot provided by W.Quayle).

# 5 Summary and Conclusions

The full $H \rightarrow ZZ \rightarrow 4l$ analysis presented in this note, shows no significant loss of sensitivity due to the increase of material upstream of the LAr Calorimeter. The 10-20% drop in signal yield with respect to the ATLAS TDR at low Higgs masses was traced in electron and muon efficiency loss during the isolation and impact parameter steps. Since the electron calorimeter isolation cuts were optimized for $p_{\perp} \geq 20$ GeV, a reoptimization of these cuts below 20 GeV is expected to recover this loss. These arguments agree with the studies performed in [3]. The extra amount of material upstream of the LAr Calorimeter increases the level of Bremsstrahlung for electrons, requiring an optimization of the tracking algorithms which will improve the impact parameter resolution. During DC1 this was not the case and a loss of efficiency in the impact parameter cut for electrons is expected. For the muon channels, a more refined Impact Parameter cut which takes into account the spread of the primary vertex in the transverse plane together with Calorimetric isolation cuts can also recover the efficiency loss. Efficiency gains at the level of 10-20% for fixed background rejections, were found in the ATLAS TDR when using these refined corrections.

The samples used in this analysis did not include electronic noise and pile-up (with the exception of the single electron samples which included both, see Appendix). For this reason, a calorimetric isolation on muons was not performed since it would have been unrealistically efficient for large cones in the LAr Calorimeter.

The author is greatful to Bill Quayle for independently cross-checking the efficiencies for all cuts and all channels, to Alden Stradling for producing the DC1 samples, to Valeria Perez Reale for pointing out the single electron samples with noise and pile-up, and to Daniel Froidevaux and Monika Wielers for stimulating discussions.

Appendix

# A Calibration Performance

The performance of the calibration described in section 3 was tested using independend electron samples (see [3] for details). In this appendix we test the performance of the new calibration on low energy electrons and $H \rightarrow ZZ^{(*)} \rightarrow e^+e^-e^+e^-$ samples. Notice that the calibration was only applied for $|\eta| < 1.37$ leading to a worse performance for electrons in the EndCap. The calibration was also used by Martina Schaefer during her $Z' \rightarrow ee$ analysis for $Z'$ masses of 200 MeV, 1.0 TeV and 1.5 TeV [9] and presented in the ATLAS overview week at Freiburg [10].

Comparison between our calibration with the default one in ATLAS is shown in figure 6 where at least the linearity of electrons coming from $H \rightarrow ZZ^{(*)} \rightarrow e^+e^-e^+e^-$ decays using the full ATLAS simulation and reconstruction is improved when compared with the current standard EMC calibration. It is also apparent that the default photon based calibration applied to electrons gives $\simeq 0.8\%$ lower energy scale.

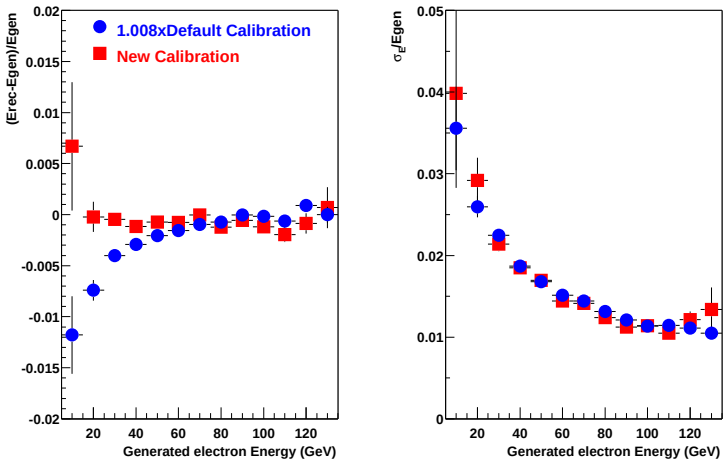


Figure 6: Electron linearity (left) and resolution (right) for the standard EMC calibration (filled circles) and a new calibration including a better treatment of upstream material. Electrons come from $H \rightarrow ZZ^{(*)} \rightarrow e^+e^-e^+e^-$ samples.

The $H \rightarrow 4e$ invariant mass distributions for Higgs masses of 130, 150, 180, 200 and 300 GeV are shown in figures 7. A comparison between the result of the present analysis and TDR is shown in figure 8.

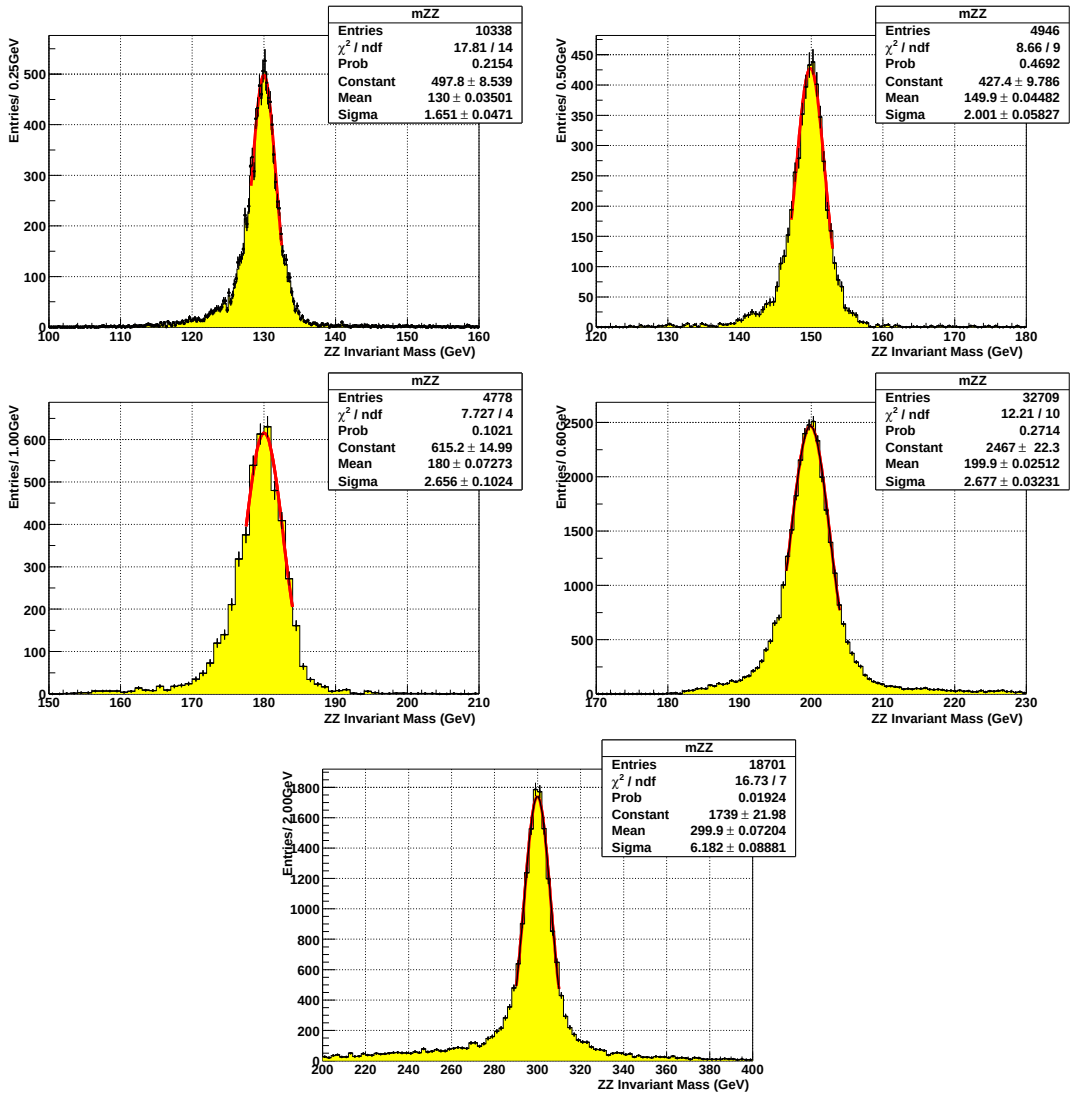


Figure 7: $H \to 4e$ invariant mass distributions for Higgs masses of 130, 150, 180, 200 and 300 GeV.

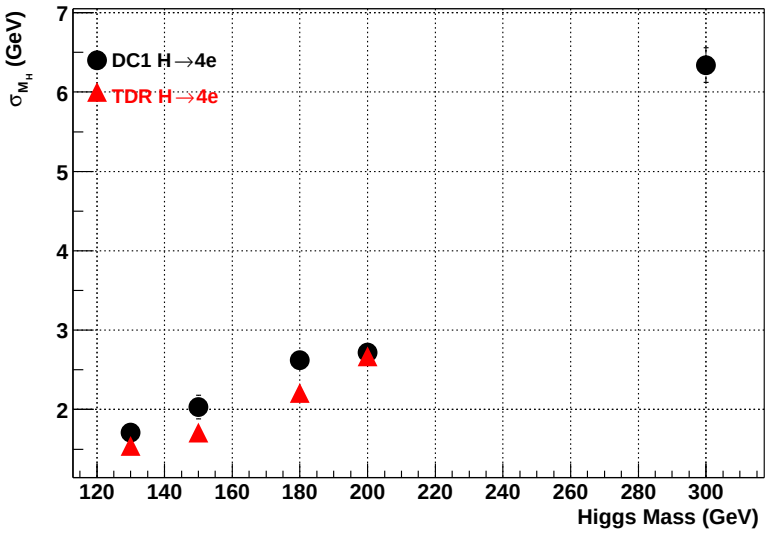


Figure 8: $H \to 4e$ invariant mass widths for the present analysis (filled circles) and the TDR (triangles) for Higgs masses of 130, 150, 180, 200 and 300 GeV.

# B Electron Efficiency Studies with FEE noise and Pile-up

In this section the single electron reconstruction efficiency after each preselection cut is presented. These electron samples include pile-up and electronics noise.

The calculation of single electron efficiencies was based on the following DC1 samples which include noise and pile-up:

```
dc1.002020.lumi02.recon.*
dc1.002024.lumi02.recon.*
dc1.002025.lumi02.recon.*
dc1.002026.lumi02.recon.*
dc1.002027.lumi02.recon.*
```

The single electron efficiencies are presented in the following set of plots which isolate the effects of separate standard selection criteria used for electrons entering the $H \to 4e$ analysis:

- Fig. 9: single electron efficiency as a function of $\eta$ for $p_\perp$ >15, 20 and 25 GeV, after EM Calorimeter clustering only.
- Fig. 10: single Electron efficiencies as a function of $\eta$ for $p_\perp$ >15, 20 and 25 GeV, after EM Calorimeter clustering and cluster-track matching.

- Fig. 11: single Electron efficiencies as a function of $\eta$ for $p_\perp$ >15, 20 and 25 GeV, after EM clustering and LAr EM isolation.
- Fig. 12: single Electron efficiencies as a function of $\eta$ for $p_\perp$ >15, 20 and 25 GeV, after EM Calorimeter clustering, LAr EM isolation and cluster-track matching.
- Fig. 13: Single Electron efficiencies as a function of $\eta$ for $p_\perp$ >15, 20 and 25 GeV, after EM Calorimeter clustering, LAr EM isolation, cluster-track matching and at least 9 hits in the Silicon detectors.

In summary from these plots we conclude that:

- a requirement of track-cluster match leads to a $\simeq$92% efficiency,
- a requirement of EM cluster isolation gives an energy dependent efficiency ranging from about 90% at 15 GeV to about 95% at 25 GeV. However there is a drop of the efficiency at for $\eta > 1.8$ where there is no presampler. There is dramatic loss of efficiency in the intercryostat (gap) region between the two calorimeters. In this region the large amount of upstream material and the sharing between the endcap and barrel calorimeters requires optimization.
- the overall single electron efficiency after all quality cuts is energy and $\eta$ dependent. It ranges from $\simeq$80% at 15 GeV to a flat $\simeq$90% at higher energies in the Barrel. In the Endcap and for $\eta > 1.8$ the efficiency drops by about 10% with respect to the barrel.

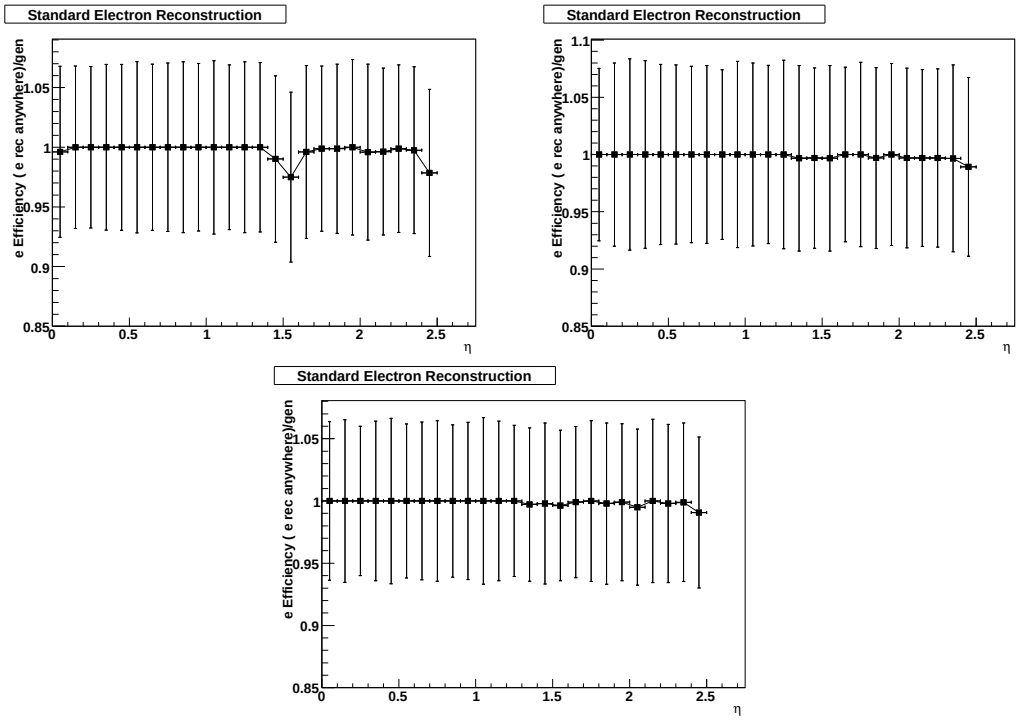


Figure 9: Single Electron efficiencies as a function of $\eta$ for $p_\perp$ >15, 20 and 25 GeV, after EM Calorimeter clustering only.

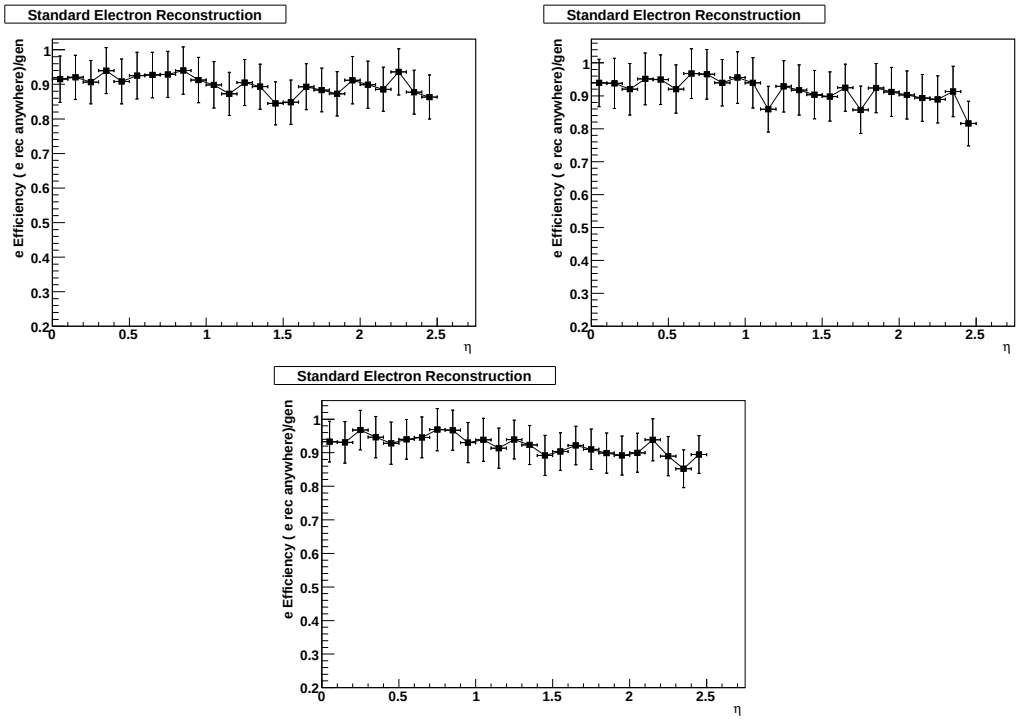


Figure 10: Single Electron efficiencies as a function of $\eta$ for $p_\perp$ >15, 20 and 25 GeV, after EM Calorimeter clustering and cluster-track matching.

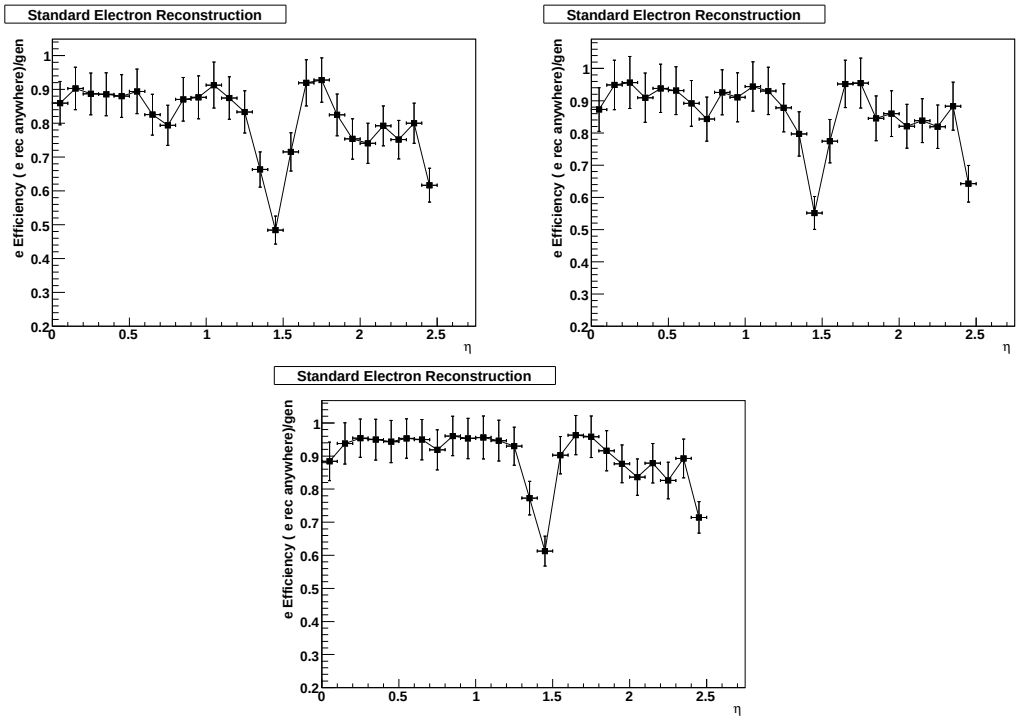


Figure 11: Single Electron efficiencies as a function of $\eta$ for $p_\perp$ >15, 20 and 25 GeV, after EM clustering and LAr EM isolation.

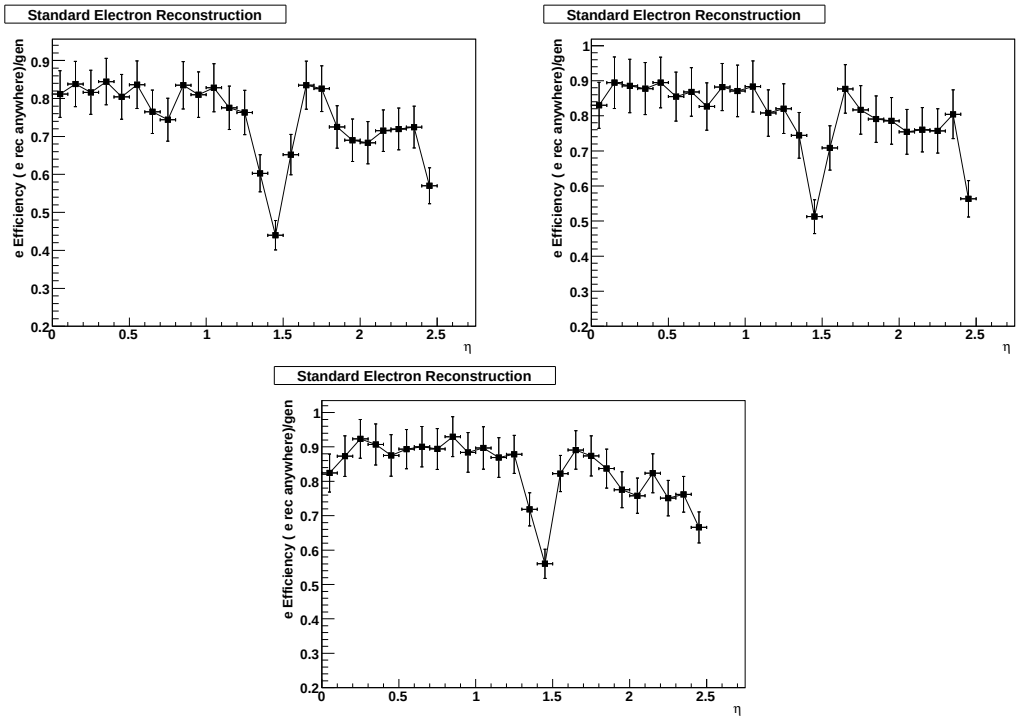


Figure 12: Single Electron efficiencies as a function of $\eta$ for $p_\perp$ >15, 20 and 25 GeV, after EM Calorimeter clustering, LAr EM isolation and cluster-track matching.

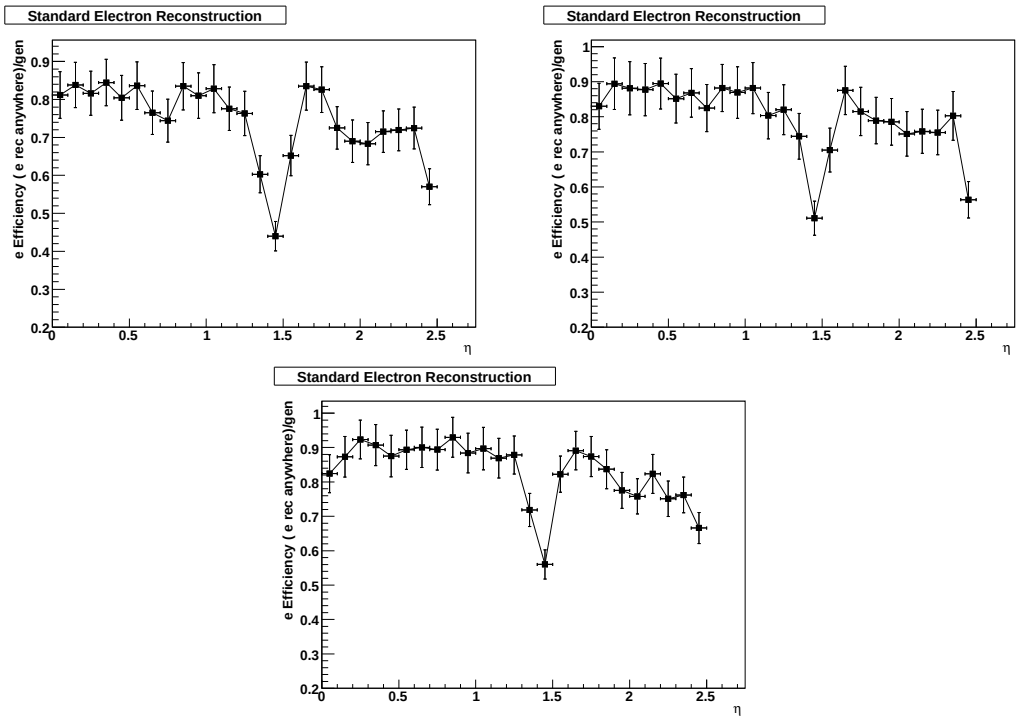


Figure 13: Single Electron efficiencies as a function of $\eta$ for $p_\perp$ >15, 20 and 25 GeV, after EM Calorimeter clustering, LAr EM isolation, cluster-track matching and at least 9 hits in the Silicon detectors.

# References


[1] J. Chollet, D. Froidevaux, S. Gadomski, L. Serin, Update on latest particle level simulations for $H \to ZZ^* \to 4l$, ATL-PHYS-93-019;
R. Hawkings, Intermediate mass $H \to 4l$: A particle level and Isolation Study, ATL-PHYS-95-062;
O. Linossier, L. Poggioli, Final State inner-bremsstrahlung effects on $H \to ZZ^* \to llll$ channel with ATLAS, ATL-PHYS-95-075;
O. Linossier, R. Zitoun, $H \to ZZ^* \to llll$ channel, in ATLAS: A complementary study of the $ZZ^*$ irrecucible background, ATL-PHYS-96-096;
O. Linossier, L. Poggioli, $H \to ZZ^* \to llll$ channel, in ATLAS. Signal reconstruction and reducible background rejection, ATL-PHYS-97-101;
G. Avolio, F. Cerutti, On the impact of the muon spectrometer alignment on the search for the SM Higgs boson in the 4mu channel, ATL-MUON-2001-01;
K. Cranmer et al, Application of K Factors in $H \to ZZ^* \to llll$ Analysis at the LHC, ATL-PHYS-2003-025;
C. Buszello et al, Prospective Analysis of Spin- and CP-sensitive Variables in $H \to ZZ^* \to l^+l^-l^+l^-$ with ATLAS, SN-ATLAS-2003-025, Eur.Phys.J., C32 (2003) 209;
T. Lagouri, Muon Combined Reconstruction $H \to ZZ^* \to 4\mu$ with MUID, ATL-MUON-2004-023;
E. Meoni.F. Cerutti, L. La Rotonda, Search for the Standard Model $H \to ZZ* \to 4$ muons with multivariate techniques and GEANT3 based detector simulation, ATL-COM-PHYS-2004-040;
B. Mellado et al, Analysis of $H \to ZZ \to 4l$ at ATLAS, ATL-COM-PHYS-2004-042.

[2] ATLAS Collaboration, Detector and Physics Performance Technical Design Report, CERN-LHCC/99-14 (1999).

[3] B. Mellado, S. Paganis, W. Quayle, Sau Lan Wu, Electron-based longitudinal weights for the ATLAS EM Barrel Calorimeter and shower isolation studies with an application to the $H \to ZZ^{(*)} \to 4e$ analysis, ATLAS Internal Note ATL-COM-CAL-2004-002, (Jul/2004).

[4] B. Anderson et al., *Phys. Rep.* **97**, 31 (1983);
T. Sjöstrand, *Comp. Phys. Comm.* **82**, 74 (1994);
T. Sjöstrand et al., *Comp. Phys. Comm.* **135**, 238 (2000).

[5] S. Frixione et al., Preprint hep-ph/0305252 (2003);
S. Frixione, B. Webber, Preprint hep-ph/0204244, JHEP 0206:029 (2002).

[6] G. Corcella et al., HERWIG 6: An event generator for hadron emission reactions with interfering gluons (including supersymmetric processes), JHEP **0101** (2001) 010; Preprint hep-ph/00011363 (2000).

[7] E. Meoni et al, ATLAS Physics Communication, ATL-COM-PHYS-2003-018 (2003).

[8] M. Wielers, ATLAS Internal Note, ATL-PHYS-99-016 (1999).

[9] Martina Schaefer, Study of $Z' \rightarrow e^+e^-$ in full simulation with regard to discrimination between models beyond the Standard Model, with Atlas, CERN.
PhD Thesis, Chapter 9.2, LPSC Grenoble, Sep/2004.
http://atlas.web.cern.ch/Atlas/documentation/thesis/thesis.html

[10] N. Kerschen, New results from e/gamma performance, talk at ATLAS Overview Week, Freiburg, Germany (Oct 5 2004).